Probing Interaction Requirements in PTP1B Inhibitors: A Comparative Molecular Dynamics Study

Rajendra Kumar, Ranajit Nivrutti Shinde, Dara Ajay, and M. Elizabeth Sobhia*

Centre for Pharmacoinformatics, National Institute of Pharmaceutical Education and Research (NIPER), SAS Nagar, Punjab 160062, India

Received December 15, 2009

Molecular dynamics studies were performed on eight different crystal structure complexes of protein tyrosine phosphatase 1B (PTP1B) to study energy components and interactions important for the binding of substrates/inhibitors. Calculation of the binding free energy and the different components was accomplished using molecular mechanics-Poisson−Boltzmann surface area and -generalized Born surface area methods. Free energy was decomposed into individual amino acid contribution to know the relative importance. Hydrogen-bond existence maps for individual ligands were monitored comprehensively. It is evident from flexibility studies that the complexes exhibit rigidity in WPD loop, which is the first prerequisite for PTP1B inhibition. The study suggests that for designing active site inhibitors, there should be an optimum balance between total electrostatic and van der Waals interactions. It is also established that for allosteric inhibitors, van der Waals interactions are significant in addition to electrostatic interactions that are responsible for strong binding affinity.

INTRODUCTION

Protein tyrosine phosphatases (PTPases) constitute a diverse family of enzymes and catalyze the selective dephosphorylation of tyrosine residue in several signal transduction processes, such as cell growth, proliferation, differentiation, and metabolism.[1] The inhibitors of PTPases are associated with many diseases including cancer, diabetes, inflammation osteoporosis, and neurodegeneration and are expected to have therapeutic effects.[2−6] PTPases have a highly conserved catalytic site consisting of 11 residue signature motif, (I/V)HCXAGXXR(S/T)G, where cysteine and arginine are essential amino acids involved in the process of dephosphorylation. Cysteine in the motif acts like a nucleophile, while arginine stabilizes the pentacovalent transition state.[7,8] Among PTPases, protein tyrosine phosphatase 1B (PTP1B), a cytosolic soluble PTPase, has shown to play a pivotal role in dephosphorylating the insulin receptor and emerged as a potential drug target for type II diabetes mellitus.[9] The knockout mice studies showed mice lacking functional PTP1B leads to insulin hypersensitivity.[10,11]

The full length of PTP1B comprises 435 amino acids constituting the major cellular form, however, only a shorter length of 298 or 321 residues is typically considered for biochemical studies. The active site of PTP1B consists of residues His214−Arg221 and loops WPD (Thr177−Pro185) and R (Val113−Ser118), which act as a gate upon ligand or substrate binding. Other important structural parts of PTP1B are S loop (Ser201−Gly209), α3-helix (Glu186−Glu200), α6-helix (Ala264−Ile281), and α7-helix (Val287−Ser295) that take part in catalysis (Figure 1). Crystallographic studies have shown that PTP1B exists in two forms, open and closed, i.e., unliganded and liganded PTP1B, respectively. The active site residues are accessible to substrate/ligand in the open form, but upon binding, conformational changes take place in the WPD, R, and S loops resulting in the closed form of the PTP1B.[12,13] Closing of the WPD loop over substrate is an important event as it brings Asp181 into a favorable position relative to ester oxygen of phosphotyrosine. It enables Asp181 to act as a general acid and base catalyst in the two step process of dephosphorylation.[14,15]

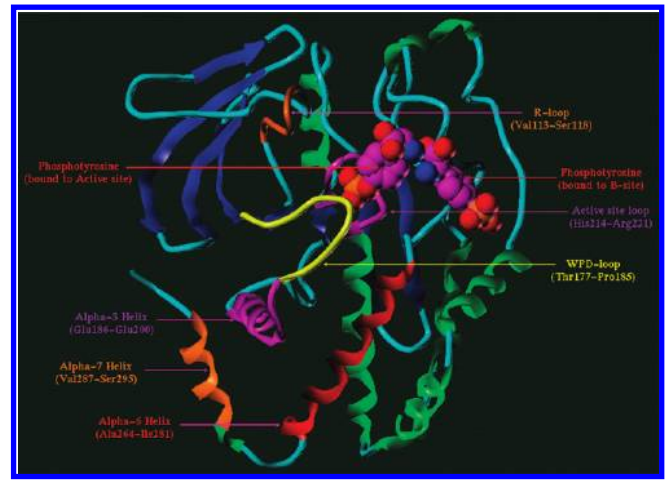

Figure 1. Structure showing important structural features of the PTP1B.

Intense research has been carried out on PTP1B and its inhibitors for the past two decades, however, none has reached the market. This is due to the selectivity and bioavailability problems associated with the hydrophilic nature of the active site and the close structural resemblance of PTP1B with its homologes. To increase the selectivity of the inhibitors, subpockets (B, C, D, and E) surrounding the active site were explored for designing potential candidates, however, most of the inhibitors developed were A and/or B

* Corresponding author. Telephone: (91) 1722214682-687. E-mail: mesophia@niper.ac.in.

10.1021/ci900484g
Published on Web 05/10/2010

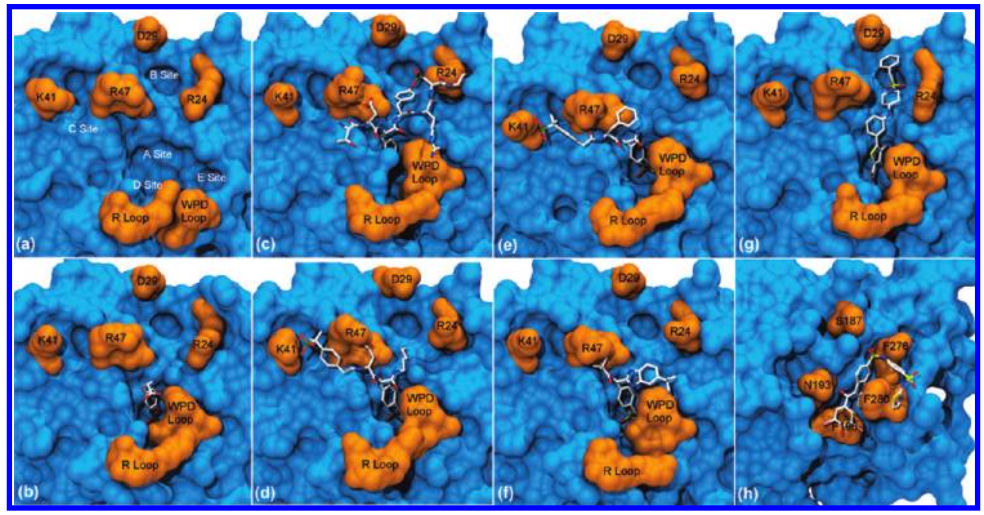

Figure 2. (a) Positions of the different binding sites surrounding the active (A site) of the PTP1B (2HNP). Binding pose of molecules in crystal structures, (b) PTP1B−phosphotyrosine complex (1PTV), (c) PTP1B IRKs activation segment complex (1G1H), (d) PTP1B−bidentate derivative (1PXH), (e) PTP1B−difluoromethylphosphonates (DFMP) derivative complex (2CNE), (f) PTP1B−nonpeptidic isothiazolidinone inhibitor (2CNG), (g) PTP1B−thiophene-2-carboxylic acid derivative complex (2QBP), (f) PTP1B−allosteric inhibitor (1T4J).

directed rather than C, D, or E sites (Figure 2a).[16] An allosteric site was explored to address this issue, and some inhibitors were also reported.[17] In addition, flexibility is a common problem in PTP1B when designing new inhibitors. Further, certain molecules show an induced fit phenomenon upon binding, making the design of new inhibitors by in silico approaches difficult.[18]

The aim of the present study is to analyze the flexibility associated with protein conformation and to study the molecular recognition between the ligands and PTP1B through molecular dynamics simulations. We have used eight crystal structures for this purpose, in which one structure is unliganded (PDB Code: 2HNP)[12] and the remaining seven are liganded structures (PDB Code: 1G1H,[9] 1PTV,[14] 2QBP,[19] 2CNE,[16] 2CNG,[16] 1PXH,[20] and 1T4J).[17] Structures 1G1H and 1PTV contain the activation segments of insulin receptor kinase (IRK) and phosphotyrosine, respectively. Structures 2QBP, 2CNE, 1PXH, and 2CNG contain inhibitors bound to A and B or to C or D sites, and 1T4J is an allosteric inhibitor complex. Figure 2 displays the position of an individual molecule into binding sites of PTP1B, while their two-dimensional (2D) structures are shown in Figure 3.

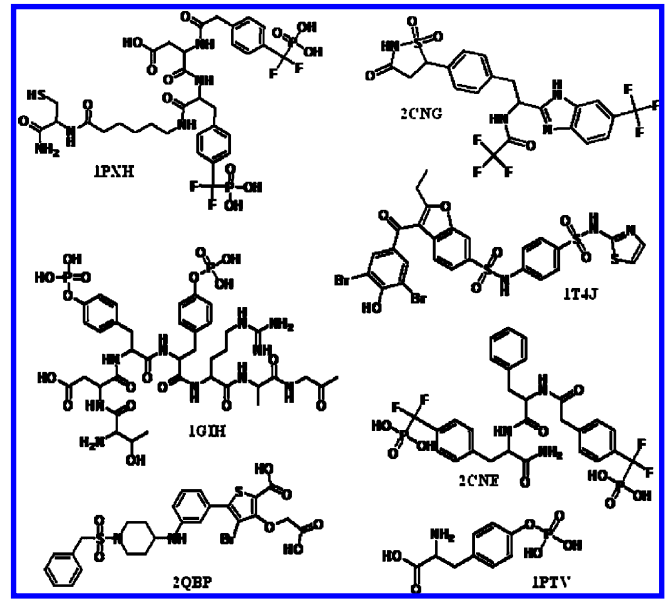

Figure 3. 2D structures of the molecules used in the study.

METHODS AND MATERIALS

A. Comparative Molecular Dynamics Simulations. Coordinates of the eight structures mentioned above were taken from the Protein Data Bank (PDB).[21] Crystallographic water molecules were removed from all the structures. Missing residues in structures 2HNP, 1G1H, 1T4J, and 2CNE were modeled using Modeler 9v7, taking 1PTV as the template.[22] The structures 1G1H and 1PTV contain mutated residues Ala215 and Ser215, respectively, which were corrected to Cys215 using Pymol's mutagenesis wizard.[23] In 1PXH, the missing coordinates of the ligand were modeled using SYBYL7.1 and a MMFF94 force field.[24] Docking was performed using AutoDock to find out the correct pose for the missing part of ligand.[25] The best pose was selected on the basis of root-mean-square deviation (rmsd) and binding free energy.

Ligands were extracted from complexes and prepared for MD studies. The structures were corrected for atom types using SYBYL7.1. The ligands were then applied with partial atomic charges derived by fitting ESP obtained by quantum electronic structure calculation. The ligands were geometry optimized with 6-31G*(p, d) basis set by the B3LYP method using the Gaussian03 program.[26] The Antechamber module was used to calculate atom centered restrained electrostatic surface potential (RESP) by fitting ESP estimated from wave functions.[27] Parameters missing for the ligands were generated using the general amber force field (GAFF) and the Parmchk module of Antechamber.[28,29] In 1G1H, the peptide contains phosphotyrosine residue, whose parameters were taken from the AMBER parameter database.[30] All structures were further processed by xLeap module of AMBER. Studies show that Cys215 and Asp181 are present as ionic and protonated forms, respectively, in physiological conditions.[31−33] Therefore for preparing the protein, the input PDB files were modified as per the requirements of the amber force field (ff03) by changing residues code CYS and ASP to CYM

and ASH, respectively. After applying the force field, all missing parts of residues and hydrogen atoms were automatically added. Structures were solvated with a TIP3P water model by creating an isometric water box, where the distance of the box is 8.5 Å from the periphery of protein.[34] Molecular systems were neutralized by the addition of counterions.

Systems were then energy minimized in two steps; in the first step, the protein and ligand were kept fixed, only the water molecules were allowed to move, and in the second step, all atoms were allowed to move. For the first step, the energy minimization was performed in 500 and 1500 steps with steepest descent and conjugate gradient methods, respectively. For the second step, the energy minimizations were performed in 1000 and 1500 steps using steepest descent and conjugant gradient methods, respectively. Heating was performed with a NVT ensemble for 10 ps where the protein−ligand complex was restrained with a force constant of 10 kcal/mol/Å^2. Equilibration has been performed for 50 ps on a NPT ensemble restraining the protein−ligand complex by 1 kcal/mol/Å^2.

Final simulations, i.e., the production phase, were performed for 2.5 ns on a NPT ensemble at 310 K temperature and 1 atm pressure. Step size was 2 fs for the entire simulation. A Langevin thermostat and barostat was used for temperature and pressure coupling. A SHAKE algorithm was applied to constrain all bonds containing hydrogen atoms.[35] The nonbonded cutoff was kept at 10 Å, and long-range electrostatic interactions were treated by the particle mesh Ewald (PME) method with fast Fourier transform grid having approximately 0.1 nm space.[36] Trajectory snapshots were taken at each 1 ps, which were finally used for analysis. All simulations were performed by the SANDER module of Amber10 with amber force field (ff03) on two processors of 3.00 GHz Intel64EMT Core 2 Duo Linux systems. Analysis was performed using VMD, GROMACS utilities, and Ptraj module of Amber tools.[30] Pymol and VMD were used for visualization purposes.[23,37]

B. Binding Free Energy Calculation. The molecular mechanics-Poisson−Boltzmann and -generalized Born surface area [MM/PB(GB) SA] methods were used to calculate binding free energy for all PTP1B complexes, using MM/PBSA implementation in AMBER10.[38−41] Binding free energy (ΔG) is given by the following equation:

$$\Delta G_{\text{binding}} = G_{\text{complex}} - (G_{\text{protein}} + G_{\text{ligand}})$$

The above equation can be written as

$$\Delta G_{\text{binding}} = \Delta G_{\text{MM}} + \Delta G_{(\text{polar,solvation})} + \Delta G_{(\text{nonpolar,solvation})} - T\Delta S$$

Where ΔG_{MM} is the molecular mechanics interaction energy between protein and ligand. ΔG_{MM} is given as

$$\Delta G_{\text{MM}} = \Delta E_{\text{int}} + \Delta E_{\text{electrostatic}} + \Delta E_{\text{vdW}}$$

Where ΔE_{int}, $\Delta E_{\text{electrostatic}}$ and ΔE_{vdW} are differences in internal, electrostatic, and van der Waals energies, respectively, in a gas phase. $\Delta G_{(\text{polar,solvation})}$ could be computed by either solving the Poisson−Boltzmann equation or using the generalized Born model. $\Delta G_{(\text{nonpolar,solvation})}$ could be estimated by following equation:

$$\Delta G_{(\text{nonpolar,solvation})} = \gamma\text{SASA} + b$$

Where γ and b are empirical constants. The γ value was set to 0.0072 kcal/mol/Å^2, while b was set to a default value of 0. SASA is the solvent accessible surface area estimated using the linear combination of pairwise overlaps (LCPO) model.[42] Entropy could be calculated by either normal-mode analysis or quasi-harmonic approximation. Estimation of entropy has been shown to be computationally expensive with a low prediction accuracy.[38,39] In this study, $T\Delta S$ was not considered for the calculation, as authors were mainly interested in protein flexibility and relative energy contribution of amino acids toward binding.

Snapshots from 0.1 to 2.5 ns molecular dynamics (MD) simulation trajectories were taken for the calculation of free energy. For PBSA and GBSA calculations, dielectric constants for solute and solvent were taken as 1.0 and 80.0, respectively. SASA was calculated using the molsurf program implemented in AMBER10 by taking the solvent probe as 1.4 Å.

C. Free Energy Decomposition Analysis. Free energy was decomposed to estimate the contribution of each residue in the binding process and was performed by using MM/PBSA of AMBER10.[43,44] Free energy was calculated by the MM/GBSA method. Energy of each residue−inhibitor interaction is given by following equation:

$$\Delta G_{\text{residue-inhibitor}} = \Delta E_{\text{ele}} + \Delta E_{\text{vdW}} + \Delta G_{\text{GB}} + \Delta G_{\text{SA}}$$

Where ΔG_{GB} is free energy due to the solvation process of polar contribution calculated using the generalized Born model. ΔG_{SA} is free energy due to the solvation process of nonpolar contribution and was calculated from SASA. MD simulation trajectories in the range of 0.1−2.5 ns were taken, and all energies were calculated for each frame. Average energy of backbone and side chains for each residue was separately calculated, and also total energy was calculated.

RESULTS AND DISCUSSION

A. Stability of Trajectories. The stability of trajectory assessed by total energy is shown in Figure 4. The graph shows the total energy curve with respect to time for all structures, where the time is from 61−2560 ps, in addition to the equilibration time of 0−60 ps which was discarded. For the structures 2HNP, 1PTV, 2QBP, 1G1H, 2CNE, 1T4J, 2CNG, and 1PXH, the average total energy (kcal/mol) is found to be −85 402.08 ± 208.55, −116 551.52 ± 234.88, −118 976.97 ± 235.06, −124 968.37 ± 238.57, −118 921.57 ± 239.73, −120 777.99 ± 241.25, −118 701.20 ± 239.06, and −121 491.01 ± 236.09, respectively. It is clear from the graph that the total energy is oscillating around the average energy, showing stability of the system at a given temperature of 310 K and a pressure of 1 atm.

To study the effective conformation sampling, the stability in terms of the rmsd was analyzed. The rmsd values for heavy atoms of all the structures were calculated by aligning all of the frames to crystal structures using the mass-weighted least-squares fitting method. The rmsd plot (Figure 5) shows the structures are stable during the course of MD simulations. However, during the production phase, the protein was allowed to move freely. The rmsd plot shows a remarkable increasing trend in the first few hundred ps of the production

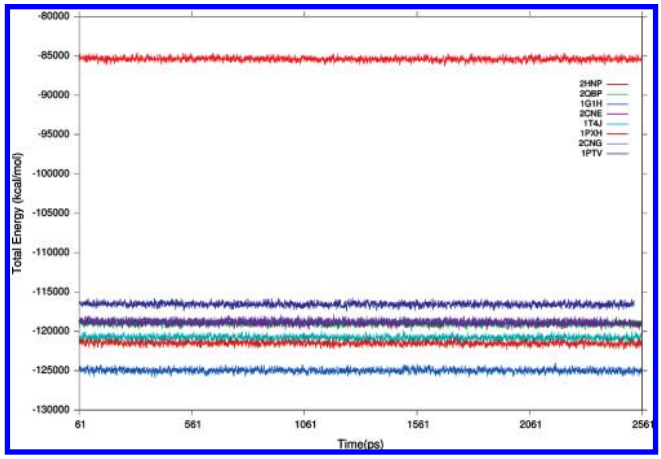

Figure 4. Total energy at each ps for different complexes in kcal/mol.

phase. This is due to the reason that the production phase was performed without restraining the proteins, whereas the equilibration phase was performed with restraints on the proteins. In 2HNP, the rmsd curve shows stability from 500 ps with the average rmsd of 1.88 ± 0.059 Å. For 1PTV, rmsd also becomes stable after 500 ps, with the average of 1.54 ± 0.058 Å. There is a different trend noticed in the rmsd of 1G1H, and it is clear from the curve (Figure 5a) that there is a slow and steady increase in rmsd from 150 to 1200 ps. It becomes stable after 1200 ps, with the average of 1.68 ± 0.074 Å. The rmsd of 1T4J shows stability after 850 ps, with the average of 1.92 ± 0.062 Å. For 2CNE and 2CNG, the rmsd becomes stable after 800 ps, with the average of 1.70 ± 0.051 and 1.49 ± 0.048 Å, respectively. In the case of 1PXH, the stability of the rmsd reaches 800 ps and continues up to 2500 ps, with the average rmsd of 1.75 ± 0.065 Å. For 2QBP, there is an increasing trend in rmsd until 950 ps and attaining stability after 950 ps, with the average rmsd of 1.75 ± 0.088 Å.

During simulation, many other parameters like volume, pressure, molecular density, temperature, and other energy components were monitored to ensure the simulation was stable. The analysis of the graphs shows that the trajectories are stable enough, and one can make use of the results for conformational sampling to calculate the binding free energy calculations.

B. Flexibility of PTP1B. Crystal structure analyses of several PTP1B bound inhibitor complexes reveal that PTP1B undergoes structural changes upon binding of different inhibitors, implying the flexibility pattern of the protein may also change upon binding to distinct inhibitors. To compare flexibility of the structures, the isotropic temperature (B) factor was determined.[45,46] The B factor is used to calculate the mobility of each residue present in a protein. It can be calculated from mean square fluctuations (msf) using the following equation:

$$B = [(8\pi^2)/3](\text{msf})$$

Mean square fluctuations were calculated for the backbone of the protein. The B factor was calculated using the equation for each residue and is plotted against each residue. Figure 6a shows the B factor plot for 2HNP, 1G1H, 1PTV, and 2CNE. The residues 41, 42, 62, 183, 185, 285, and 288 of 2HNP show more flexibility in comparison to 1G1H, 1PTV, and 1T4J, which is expected due to its unliganded form. The loops containing these residues exhibit flexibility. The WPD loop showed rigid movement in 1G1H and 1PTV making interactions with the atoms of ligands. On the other hand, in the case of allosteric inhibitor, there are restrictions in the WPD loop movement which blocks the catalysis and causes finally the inhibition of PTP1B. In the case of the R loop, the flexibility seems to be more in 1T4J than in 2HNP due to the direct influence of the WPD loop movement on the R loop. In 1G1H, the flexibility in the R loop is caused by Lys116 that is present on the outer side of the protein and is exposed to solvent. In the open unliganded form, Lys116 shows interaction with WPD loop residues viz., Asp181 and Phe182, and lies between the WPD loop and the active site, making itself suitable for catalysis. Lys116 should be moved, making it like a gate for the active site. 1PTV shows the same trend of flexibility as that of 1G1H except with the R loop, in which Asp181 interacts with Lys116. The WPD loop is rigid in this structure, which in turn makes Asp181 rigid. The interaction of Asp181 with Lys116 makes the R loop rigid. The structure 2QBP has a different type of flexibility pattern, as shown in Figure 6b. The residues Asp181 and Phe182 of the WPD loop exhibit more flexibility as compared to those of 1G1H and 2CNE. Residue 27, 28, and 29 of the B site were affected in case of 2QBP, as it is showing large flexibility with respect to 1G1H. Ligand interaction in 2QBP is not favorable because of the flexibility in the WPD loop and the B site. 2CNE and 1G1H show the same flexibility trend except the R loop, where the flexibility is more pronounced in the latter case.

In 1PXH, the ligand binds to both B and C sites, which is reflected in the flexibility graph. Clearly, the residues 27−29 of the R loop show high flexibility (Figure 6b). In addition, the loop containing Thr165 also shows more flexibility when compared to 2HNP. 2CNG shows the same flexibility pattern as that of 1G1H except for the R and S loops, which are more flexible in the case of 1G1H. The WPD loop for both 1PXH and 2CNG show more rigidity as compared to 1G1H.

Overall one can say that all of the PTP1B inhibitor complexes exhibit rigidity in the WPD loop, which is the first essential requirement for PTP1B inhibition. The R loop is flexible only in case of 1G1H and 1PXH, and this may be due to the extensive binding of the ligand to both the B and C subpockets. The S loop has the same flexibility pattern in 2HNP, 1PXH, and 1G1H but is more produced when compared to other structures. However, among all the structures, 1PTV has the highest flexibility in the S loop.

C. Binding Free Energy. Binding affinity of ligands can be studied on the basis of binding free energy, which is estimated using the MM-PBSA and -GBSA methods. In the present study, we estimated the different components of interaction energy that contribute to binding. These include van der Waals, electrostatic, polar solvation, and nonpolar solvation interaction energies. Here the entropy was not calculated, as we are only interested in the relative binding free energy. Table 1 shows the binding free energy of all the complexes with their energy components.

A lower value of ΔG_{total} was noted for 1G1H compared to the other complexes, which is probably due to the presence of IRK's activation segment peptide. For 1GIH, the electrostatic contribution is very high, as shown by its low value (Table 1), owing to the presence of two phosphates in the

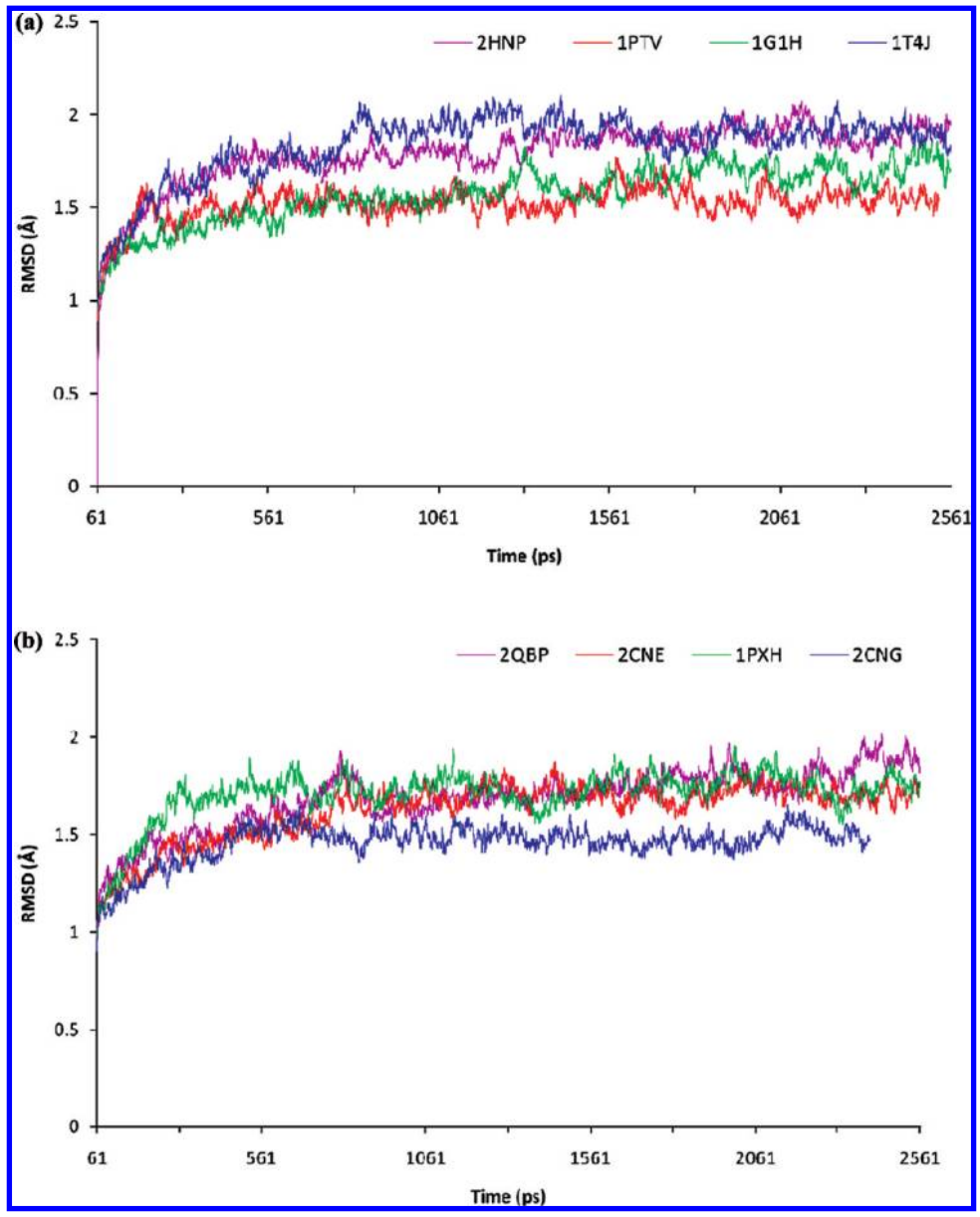

Figure 5. (a) Plot of the rmsd with respect to time for 2HNP (magenta), 1PTV (red), 1G1H (green), and 1T4J (blue). (b) Plot of the rmsd with respect to time for 2QBP (magenta), 2CNE (red), 1PXH (green), and 2CNG (blue). Rmsd is calculated for heavy atoms with reference to their respective crystal structure.

peptide, and the polar solvation is low, as reflected by its higher value. The sum of the electrostatic component of the molecular mechanics energy and the electrostatic contribution of solvation ($\Delta E_{\text{elec-total}}$) is found to be favorable for binding. Moreover, in 1G1H, the higher negative value of van der Waals interaction and the nonpolar component of the solvation energy correspond to a favorable stronger binding when compared to rest of the complexes. In 1PTV, the $\Delta E_{\text{elec-total}}$ interaction energy appears to follow the same trend as that of 1G1H. Due to the presence of only one phosphate group in the structure, the electrostatic contribution is found to be less than that of 1G1H. The van der Waals contribution is lower than that of 1G1H. In this structure, the electrostatic contribution is more favorable and the van der Waals contribution less favorable than 1GIH, which makes the phosphotyrosine binding affinity lesser than IRK's activation segment peptide. Because of this, 1G1H showed a free energy of -98.39 ± 14.24 (PBSA) and -102.63 ± 14.22 (GBSA), while 1PTV showed -50.17 ± 6.34(PBSA) and -51.15 ± 5.92(GBSA). This is concurrent with experimental findings, where 1GIH is binding much stronger than 1PTV (Table 1).

For structure 2QBP, the $\Delta E_{\text{elec-total}}$ has a positive value, which corresponds to the unfavorable binding of the ligand. As the ligand is neutral, ΔE_{elec} is relatively very high compared to that of 1G1H, and the binding is favored only by van der Waals and nonpolar interactions. Also, ΔG_{total} shows the ligand is bound with very low affinity. In 2CNG, the electrostatic contribution is low due to which $\Delta G_{\text{polar,solvation}}$ and $\Delta E_{\text{elec-total}}$ also become low, as compared to 2QBP. Hence, the ligand bound to 2QBP has lower binding affinity than 2CNG.

The structures 1PXH and 2CNE contain ligands that have two phosphate groups which bind to different sub pockets of the protein. In 1PXH, the ligand contains an additional charged carboxyl group. Comparing 1PXH and 2CNE, the

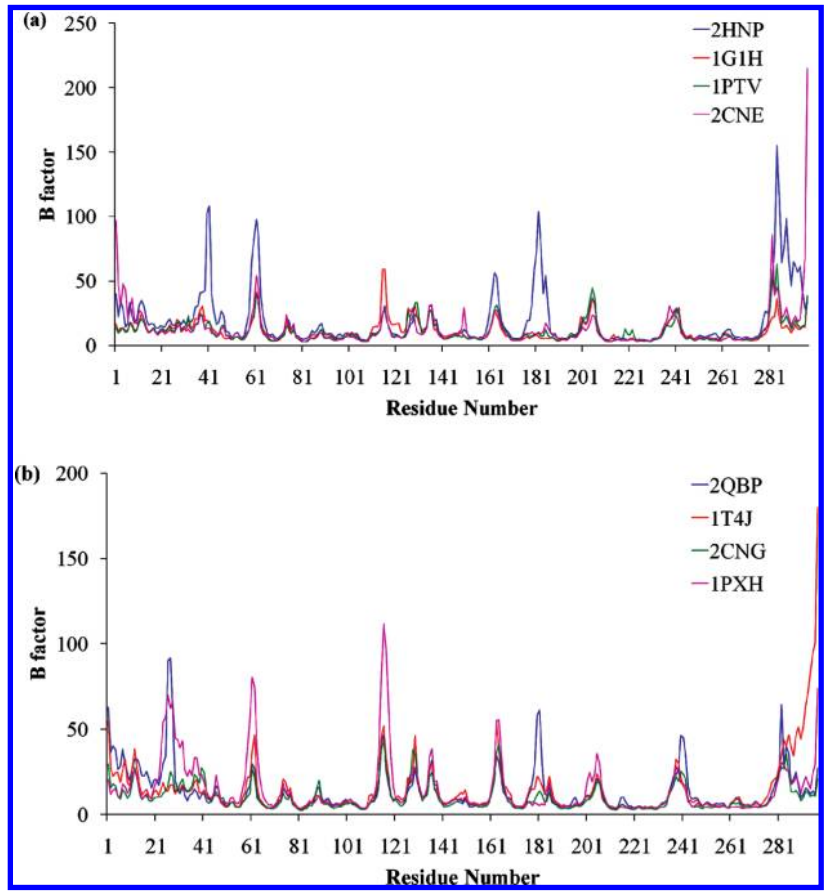

Figure 6. (a) *B* factor plot for 2HNP (blue), 1G1H (red), 1PTV (green), and 2CNE (magenta). (b) *B* factor plot for 2QBP (blue), 1T4J (red), 2CNG (green), and 1PXH (magenta). *B* factor is calculated from the mean square fluctuations of backbone atoms.

Table 1. Binding Free Energy and Its Components for All Complexes

interaction energy (kcal/mol)	1PTV	2QBP	1G1H	1T4J	2CNE	2CNG	1PXH
inhibition activity	k_m = 5 mM[14]	K_i = 4nM[19]	K_Ms = 14 μM[9]	IC_{50} = 8 μM[17]	IC_{50} = 1.7nM[16]	IC_{50} = 110nM[16]	K_i = 1.8nM[20]
ΔE_{elec}	−299.66	−29.41	−617.85	−7.9	−523.67	−33.72	−564.21
ΔE_{vdW}	−22.08	−46.47	−63.08	−60	−41.47	−40.84	−58.49
$\Delta G_{nonpolar,solvation}$ (PBSA)	−3.72	−6.24	−9.83	−6.59	−6.49	−5.04	−9.19
$\Delta G_{polar,solvation}$ (PBSA)	275.28	63.77	592.37	34.31	511.9	47.04	544.36
$\Delta E_{elec\text{-}total}$	−24.38	34.36	−25.48	26.41	−11.77	13.32	−19.85
ΔG_{total} (PBSA)	−50.18 ± 6.34	−18.35 ± 5.96	−98.39 ± 14.24	−40.18 ± 4.15	−59.73 ± 7.72	−32.56 ± 4.89	−87.53 ± 10.13
$\Delta G_{nonpolar,solvation}$ (GBSA)	−3.72	−6.24	−9.83	−6.59	−6.49	−5.04	−9.19
$\Delta G_{polar,solvation}$ (GBSA)	274.31	47.97	588.13	30.29	513.76	38.41	546.26
ΔG_{total} (GBSA)	−51.15 ± 5.92	−34.15 ± 6.10	−102.63 ± 14.22	−44.2 ± 3.53	−57.87 ± 6.39	−41.19 ± 4.49	−85.63 ± 8.15

electrostatic contribution is more in 1PXH than in 2CNE, which is due to the presence of an extra charged group in 1PXH. In addition, the $\Delta E_{elec\text{-}total}$ is also lower in 1PXH as compared to 2CNE. The higher contribution of electrostatic interaction, van der Waals, and nonpolar solvation components primarily contributes to the stronger binding affinity in 1PXH as compared to 2CNE. The binding free energy (GBSA and PBSA) for 2CNG (IC_{50} = 110nM) and 2CNE (IC_{50} = 1.7nM) follows the trend of experimental IC_{50} in (Table 1). Also in case of inhibitors 1PXH (K_i = 1.8nM) and 2QBP (K_i = 4nM), the same fold of increment in free energy as that of experimental affinity (∼2.2) is observed for both methods (GBSA and PBSA) (Table 1).

The analyses show there should be a balance between total electrostatic and van der Waals interactions for effective binding. Though electrostatic interactions play a vital role in binding, the high electrostatic potential leads to a higher charge density, which affects the bioavailability of the molecules. Therefore, it is essential to keep the electrostatic contribution at the optimum level. In the active site directed complexes, the presence of charge on the inhibitors becomes an essential prerequisite for binding, as the active site is also charged. But van der Waals interaction becomes more important when the inhibitors have lower electrostatic contributions. The analyses show the molecule with moderate electrostatic contributions with a negative total electrostatic

Table 2. PDB Entries and Hydrogen-Bonds Monitored for Each Ligand in the Dynamic Study

PDB id	Hydrogen bonds monitored	PDB id	Hydrogen bonds monitored
1PXH	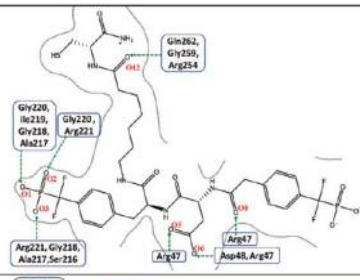	1G1H	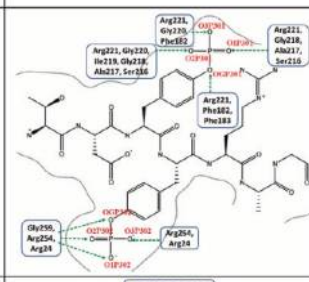
2QBP	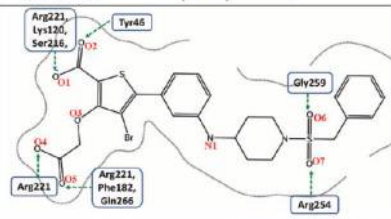	2CNG	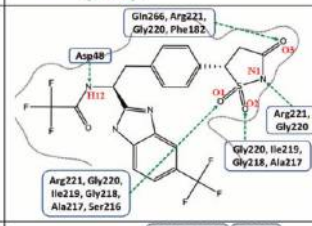
1T4J	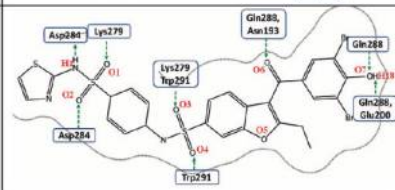	1PTV	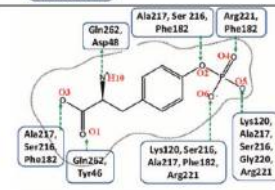
2CNE	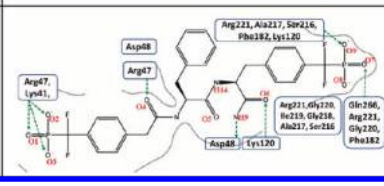		

energy and higher van der Waals interaction may have good binding affinity. It also shows any new molecule that has an equivalent $\Delta E_{\text{elec-total}}$ of 1PTV and ΔE_{vdW} of 1PXH can show a higher binding affinity.

1T4J contains an allosteric inhibitor which is neutral in nature, as a result of which electrostatic contribution is not favorable for binding and also shows high fluctuation. On the other hand, binding is favored by van der Waals and non polar interactions. Binding free energy for the ligand by PBSA and GBSA was found to be -40.18 ± 4.15 and -45.15 ± 3.5, respectively. Computational study has revealed the benzofuran moiety of an inhibitor makes hydrophobic interactions with the hydrophobic core (Trp291, Phe280, Phe196, and Leu192).[47] In concurrence with this study, our results also demonstrate that van der Waals interactions ($\Delta E_{\text{vdW}} = -60$, Table 1) provide the highest contribution toward binding free energy. Thus, hydrophobic interactions seem to play a more important role than electrostatic for allosteric inhibitors to improve binding affinity.

D. Binding Contribution and Interactions. Molecular recognition is an important process in receptor−ligand binding, and one can analyze different types of interactions by making use of the three-dimensional structures. The comparative crystal structure analysis can provide an understanding of interactions which are important for formation of substrate/inhibitor complexes. In this study, we have analyzed the interaction in the dynamic environment, where the interactions depend on time, to get more insight into molecular recognition. Interactions were analyzed on the basis of free energy decomposition and hydrogen-bond analysis. For each complex, free energy was decomposed to analyze contribution of individual residues in binding. The hydrogen bonds which showed stable behavior during molecular dynamics were analyzed in detail. Stable hydrogen bonds with water molecules were also analyzed to find out the importance of water molecules in ligand−protein interactions. Hydrogen bonds between ligands and proteins that were monitored throughout the simulation time are shown in Table 2. Original hydrogen-bond existence maps are given as Supporting Information. Refer to Table 2 for the explanation of hydrogen-bonding interactions of individual complexes.

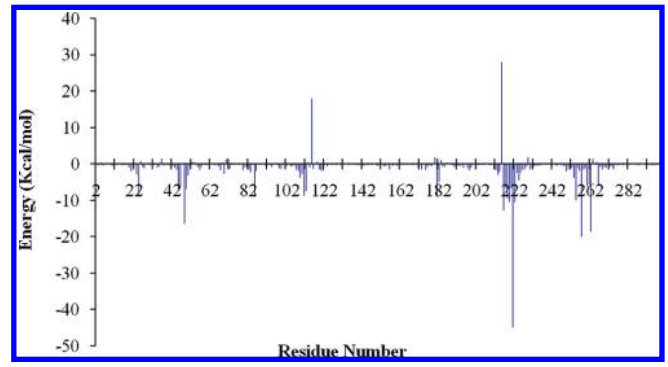

Figure 7. Free energy decomposition plot for 1G1H. Cys215 and Lys120 oppose binding, while Arg220 and others with negative energy favor binding.

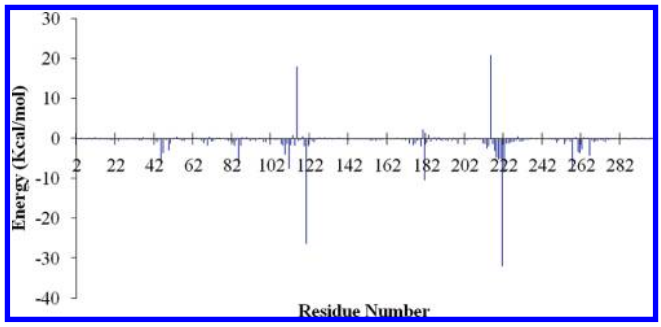

Figure 8. Free energy decomposition plot for 1PTV. Cys215 and Glu116 oppose binding, while Arg221 and Lys120 favor binding.

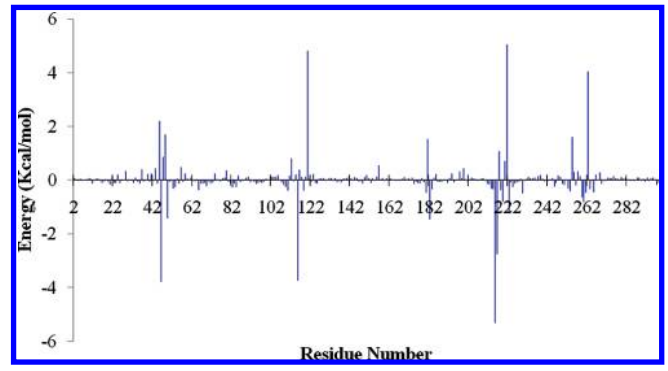

Figure 9. Free energy decomposition plot for 2QBP. Cys215 favors binding, while Arg221 opposes binding.

i. PTP1B−IRKs Activation Segment Complex (1G1H). Figure 7 shows the total free energy contribution with respect to residue number, where total free energy includes van der Waals, electrostatic, and solvation free energies. For analysis, bothof the phosphotyrosine groups were considered, as these show higher contribution in binding free energy. The residues Glu116 and Cys215 show high positive energy values, indicating that these two residues are unfavorable for binding, which was confirmed by flexibility analysis that the R loop has high mobility which is not suitable for binding. Cys215 has a negative charge and is close to the phosphate group of first phosphotyrosine, which is also negatively charged making it highly unfavorable for binding. However, favorable interactions from Ser216 to Arg221 also stabilize the binding of phosphotyrosine, despite the presence of an anionic (thiolate) form of Cys215. In the B site, the residues Arg24, Arg257, and Gln262 show positive contribution and exhibit favorable binding for the second phosphotyrosine residue of the peptide.

It is interesting to note from the hydrogen-bond existence map, (see Supporting Information) many of the residues that are favorable for binding, as per free energy contribution, are also found to be involved in the hydrogen bonding. The active site residues Ser216 to Arg221 form hydrogen bonds with the oxygen atoms of phosphate group. Ser216 to Ile219 show a single hydrogen bond with the first phosphotyrosine residue. Arg221 is involved in the formation of three hydrogen bonds simultaneously with the phosphate group that corresponds to strong interactions. Phe181 of the WPD loop also forms a stable hydrogen bond with the phosphate group making it rigid and in closed form. Arg24 and Arg254 are favorable as they form hydrogen bonds with the phosphate group of second phosphotyrosine groups. Arg24 and Arg254 are involved in one and two hydrogen bonds, respectively. Asp48 is also an important residue which forms two stable hydrogen bonds with a peptide backbone and exhibits a positive contribution in free energy of binding. Asn85, Arg257, and Gln262 have positive contributions in binding, but these three residues do not show any hydrogen-bond interactions.

Comparison of flexibility studies with binding free energy calculations shows the residues with high mobility show unfavorable binding in free energy calculations. For example, Glu116 shows a high mobility which is not favorable for binding. All the active site residues, except Cys215, are favorable for binding, however, due to the rigid nature of the active site, Cys215 also becomes rigid. Overall, residues which are favorable for binding also show rigidity in movement.

ii. PTP1B−Phosphotyrosine Complex (1PTV). The binding free energy contribution plot (Figure 8) shows that a number of contributions in 1PTV are less than that of 1G1H. This is because the inhibitor is active site bound and contains only one phosphate group. The residues Glu116 and Cys215 show a positive interaction energy which is unfavorable for binding. Lys120 is very favorable for binding and assists in surmounting the negative contribution of Glu116 (R loop). Arg221 shows a high-positive contribution in binding which overcomes the negative contribution of Cys215. Active site residues have less contribution as compared to 1G1H. Asp181 of the WPD loop also shows a positive contribution in the binding of phosphotyrosine. Arg257 and Asn111 are favorable for binding, whereas Gln262 shows very little contribution in binding phosphotyrosine.

Hydrogen-bond existence map shows that many interactions of second phosphotyrosines are absent or very weak in this complex, as compared to the first phosphotyrosine residues of 1G1H. The active site residues, Ser216, Ala217, and Arg221 are involved in stable hydrogen-bonding interactions. Arg221 shows three hydrogen-bond interactions simultaneously that are responsible for stabilizing the phosphate group in the active site. Phe182 forms a stable hydrogen bond and is responsible for the rigidity of the WPD loop in addition to the contribution of Asp181. Lys120 of the R loop forms a stable hydrogen bond with the phosphate group and is responsible for the rigidity of the R loop.

iii. PTP1B−Thiophene-2-carboxylic Acid Derivative Complex (2QBP). Compared to 1PTV and 1G1H, the binding free energy contribution plot for this ligand is found to be different (Figure 9). It also has the lowest binding free energy among all complexes. Individual amino acid contribution in terms of energy is also very low (±10 kcal/mol). Cys215 and Ser216 are favorable for binding because of the presence of a carboxylic acid group in place of the phosphate group. Asp48 shows a negative contribution to binding and is unfavorable for interaction.

The hydrogen-bond existence map shows less frequent interactions of the ligand with the protein. A similar study has been carried out by Wang et al., where 10 ns MD simulations of 2QBP are performed using GROMACS 3.3.1.[48] It is observed that the WPD loop of 2QBP is less flexible with respect to uncomplexed proteins. In addition, the thiophene moiety of the inhibitor makes constant hydrogen-bonding interactions with active site amino acids, like Ser216, Ala217, Gly218, Ile219, and Arg221. Our results were found to confer with the above, as the WPD loop amino acids also are found to be more rigid compared to that of 2HNP (Figure 6a). Moreover, Ser216 and Arg221 were found to evidence intermittent interactions with an inhibitor. Other

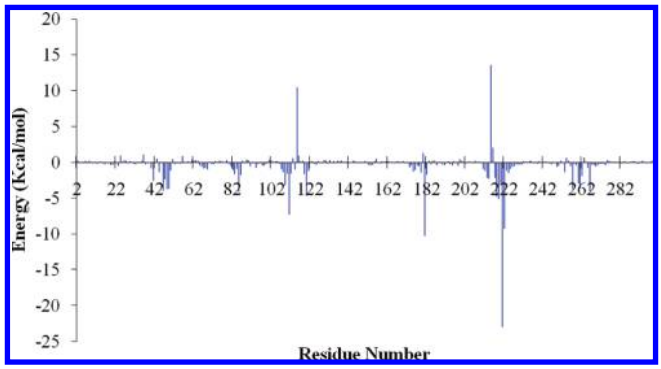

Figure 10. Free decomposition plot for 2CNE. Cys215 and Glu116 oppose binding, but Ser220, Arg221 and Phe181 favor binding of an inhibitor.

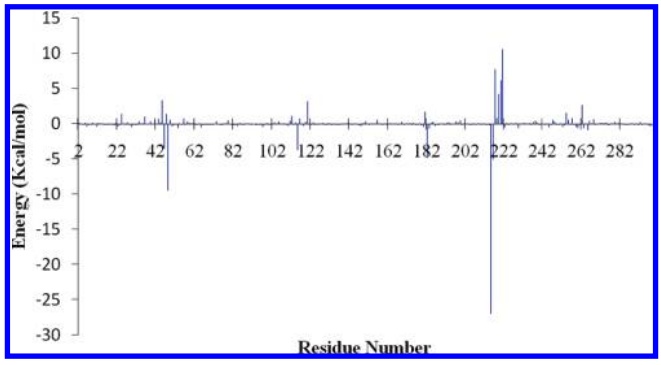

Figure 11. Free decomposition plot for 2CNG. Ser220 and Arg221 oppose binding, but Cys215 and Tyr46 favor binding of inhibitor.

bondings were found to be less frequent. Absence of these interactions can be attributed to the use of different simulation methods (GROMACS/Amber) and to the length of the run (10 ns/2.5 ns).

iv. PTP1B−DFMP Derivative Complex (2CNE). Binding free energy contribution from residues (Figure 10) is approximately the same as that of PTP1B−phosphotyrosine complex. The residues Arg221 and Ser222 contribute positively for binding and overcome the unfavorable contribution caused by Cys215. Also, Phe182 of the WPD loop contributes to the binding. Gln111 and Lys120 also favor binding of the ligand in the active site pocket. In C sub pocket, Tyr46, Asp48, and Val49 show a positive contribution in binding.

The two residues, Ser216 and Arg221, from the active site loop are involved in formation of stable hydrogen bonds. Arg221 makes a strong hydrogen-bond interaction with a phosphate group. Phe182 is involved in hydrogen-bond formation, causing rigidity of the WPD loop. In C sub pocket, two residues are involved in the formation of hydrogen bonds. Arg47 forms two hydrogen bonds with the second phosphate group, while Lys41 forms one hydrogen bond.

v. PTP1B−Nonpeptidic Isothiazolidinone Inhibitor (2CNG). Figure 11 shows a different trend of free energy contribution for the active site residues. Many of the active site residues, including Arg221, are not favorable for binding. Due to a high positive contribution of Cys215, the ligand has favorable binding toward the active site. In the case of the R loop, the trend is opposite, where Lys120 shows negative contribution toward binding, but Glu116 favors the binding of the ligand. Also Tyr46 and Asp48 contribute favorably to the binding of the ligand.

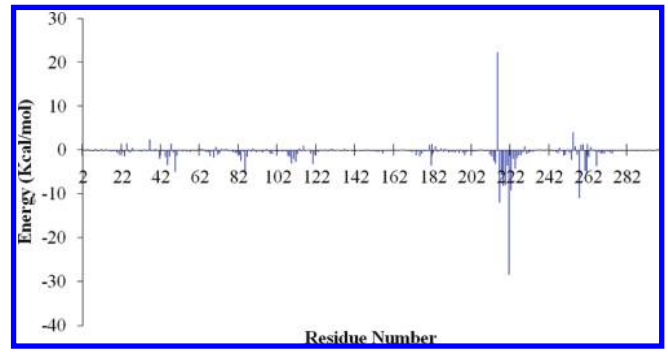

Figure 12. Free decomposition plot for 1PXH. Active site residues, except Cys215, favor the binding of an inhibitor.

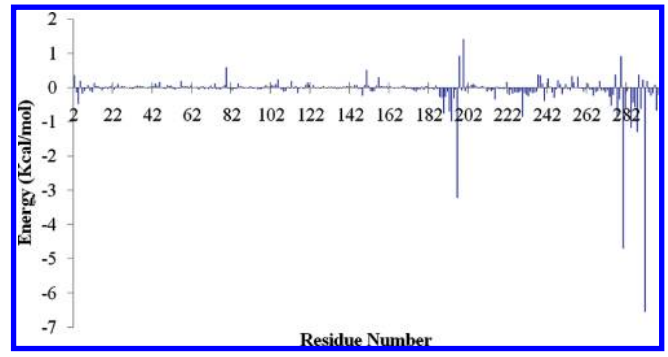

Figure 13. Free decomposition plot for 1T4J. Electrostatic contribution is low and not significant.

From the hydrogen bond existence map, it is found that two active site loop residues, Ala217 and Arg221, are involved in forming stable hydrogen bond interactions. Other active site loop residues are involved in weak interactions, which are not stable during simulation. Also, Asp48 shows stable hydrogen bonding during simulation.

vi. PTP1B−Bidentate Derivative (1PXH). The free energy decomposition pattern (Figure 12) for active site residues is similar to that of 1G1H. In site B, Arg257 shows a positive contribution, while Gln262 shows a negative contribution. In this complex, the contribution of Arg24 of the active site and the contribution from the R loop are absent. So the contribution seems to be totally from the active site and the sub pocket B. Although the ligand is present in the site C, there are no significant contributions noticed from the site C.

From the hydrogen-bond existence map, it is studied that all active site residues, including Ser216 to Arg221, are involved in strong hydrogen-bond interactions, as seen in 1G1H. In sub pocket B, the residues Arg24 and Arg254 do not interact with the ligand through hydrogen bonding, and no other stable hydrogen-bond interactions are noted in this pocket. In sub pocket C, Lys41 is involved in hydrogen-bond interactions, but Arg47 does not make any interactions. It is interesting to note that the ligand exhibits the second highest binding free energy, though it does not show any strong interactions with the B and C sub pocket residues.

vii. PTP1B−Allosteric Inhibitor (1T4J). Figure 13 shows the free energy decomposition plot for the allosteric inhibitor complex. It shows the contribution of each residue in binding of the ligand. Residues Phe196, Phe280, and Trp291 contribute strongly for the binding through van der Waals interaction energy. Other residues which are involved in positive contribution of binding are Phe191, Gly277, Asp284,

and Val287. From the hydrogen-bond existence map, it is found that only one hydrogen-bond interaction is present, which is between Asp283 and oxygen of a sulfo group. This interaction together with the hydrophobic interactions from Phe196, Phe280, and Trp291 are responsible for the stability of the ligand between two helices.

From the above analyses, one can understand that the active site interactions are primarily important for higher binding affinity, as supported by the experimental result.[16] In complexes containing the phosphate group in the active site, a similar trend is seen. The binding is opposed by Cys215, but interactions are stabilized by Arg221, which are in line with the experimental findings.[7,31,38] The analysis also shows strong binding affinity, interactions within the active site should be stable. For example, in 1G1H and 1PXH, the active site hydrogen-bond interactions are very stable and also have a similar trend in binding free energy decomposition. In other complexes, many of these hydrogen-bond interactions are absent or weak during the course of simulations, and the contributing residues are also found to be different. A comparison of the hydrogen-bonds interactions with binding free energy revels that the complexes having more numbers of hydrogen bonds in the active site correspond to a higher binding affinity. Asp48, Lys120, and Phe182 are three other important residues responsible for stabilizing the ligand in the active site. Collectively, electrostatic interactions are the drivers of binding affinities, as also observed by Zhang et al., in docking and subsequent MD studies of structurally diverse PTP1B inhibitors, where by the weight increment of electrostatic component from 1.0 to 1.2 in GAFF force field established stability in MD simulations.[49] In view of the qualitative comparison, high-electrostatic contributions toward binding free energies of ligands in our studies (Table 5) is in agreement with Zhang et al. findings and reemphasizes the role of electrostatic interactions in PTP1B active site inhibitors.

For selectivity, interactions in surrounding sub pockets are required, and it has little effect on binding affinity. B sub pocket residues Arg24 and Arg254 are important and are involved in hydrogen bonding. From the free energy decomposition plot, it has been found that Arg257 and Gln262 are also important interacting residues. In the C sub pocket, Arg47 and Lys41 are important residues involved in interaction. After comparing the binding free energy and the hydrogen-bonding interaction of 1PXH and 2CNG, it has been found that there are strong interactions in the B site, as compared to C site. Hence for selectivity, the B site is more favorable, as compared to the C site, and can be used to design new inhibitors.

In the case of allosteric inhibitors, hydrophobic interactions are more important than hydrophilic interactions. Three important residues Phe196, Phe280, and Trp291 are hydrophobic residues involved in interactions. In crystal structures, three residues Asn193, Glu276, and Lys279 are involved in hydrogen-bonding interactions. But during simulations, all these interactions cease to exist, and only Asp284 was found to be involved in hydrogen-bonding interactions. This hydrophilic interaction has an important role in stabilization of the inhibitor. During simulation, it has been found that there is displacement of α-7 helix, and it creates a place for the inhibitor between the α-7 and the α-6 helix. It stabilizes inhibitors between both helices, and it has been found that the benzofuran ring of inhibitor is always sandwiched between Phe280 and Trp291.

CONCLUSIONS

Eight different crystal structure complexes of protein tyrosine phosphatase 1B (PTP1B) were studied with molecular dynamics. In the amino acid flexibility analysis, the WPD loop has been found to be rigid in the seven complexes compared to uncomplexed protein. This is an essential event which might be required for substrates to get dephophorylated, while it provides affinity for inhibitors over substrates to act as competitive inhibitors. In addition, Lys116 is another residue which shows a contrast flexibility pattern compared to the eight complexes. It acts as a gatekeeper where it makes interactions with the Asp181 of the WPD loop in an open structure and becomes intermittent after binding of inhibitors. Binding energy calculations show that binding affinity of substrates/inhibitors (active site) is mostly driven by electrostatic interactions contributed by Ser216 to Arg221, Asp48, Lys120, and Phe182. Most of them are the hydrogen bonding and provide strong binding. Cys215, present as the thiolate form, has been found to be unfavorable for binding of the phosphate group containing substrates/inhibitors. The contribution of van der Waals interactions toward binding was found to be less. PTP1B with a B site inhibitor has more binding affinity than that of a C site inhibitor. In both B and C sites, electrostatic interactions play a vital role. In the B site, important residues involved in interactions are Arg24, Arg254, Arg257, and Gln262, whereas in the C site, important interacting residues are Arg47 and Lys41. It is noted that there should be an optimum balance between total electrostatic and van der Waals interactions while designing active site directed inhibitors. Also inhibitors can be modified to improve interactions with thiolate Cys215.

In the case of allosteric inhibitors, electrostatic interactions do not contribute significantly toward binding, but van der Waals contributions are predominant. There are strong hydrophobic interactions present between the benzofuran ring of the allosteric inhibitor and the residues Trp291 and Phe280, but Asp284 is the lone residue interacting through a hydrogen bond. Only a few hydrogen-bonding interactions make ligands bind with lower affinity. Electrostatic interactions can be exploited for obtaining a strong binding affinity.

ACKNOWLEDGMENT

The authors thank the Department of Science and Technology (DST) and the Council of Scientific and Industrial Research (CSIR), New Delhi, India for financial assistance.

Supporting Information Available: Hydrogen bonds monitored for each molecule (Table 2 in text) during simulation time are provided in Figures 1−7. This information is available free of charge via the Internet at http://pubs.acs.org/.

REFERENCES AND NOTES

(1) Hunter, T. Signaling and Beyond. *Cell* **2000**, *100*, 113–127.

(2) Andersen, J. N.; Jansen, P. G.; Echwald, S. M.; Mortensen, O.; Fukada, T.; Del Vecchio, R.; Tonks, N. K.; Moller, N. P. H. A Genomic Perspective on Protein Tyrosine Phosphatases: Gene Structure, Pseudogenes, and Genetic Disease Linkage. *FASEB J.* **2004**, *18*, 8–30.
(3) Arena, S.; Benvenuti, S.; Bardelli, A. Genetic Analysis of the Kinome and Phosphatome in Cancer. *Cell. Mol. Life Sci.* **2005**, *62*, 2092–2099.
(4) Bialy, L.; Waldmann, H. Inhibitors of Protein Tyrosine Phosphatases: Next Generation Drugs. *Angew. Chem., Int. Ed. Engl.* **2005**, *44*, 3814–3839.
(5) Van Huijsduijnen, R. H.; Bombrun, A.; Swinnen, D. Selecting Protein Tyrosine Phosphatases as Drug Targets. *Drug Discovery Today* **2002**, *7*, 1013–1019.
(6) Zhang, Z. Y. Protein Tyrosine Phosphatases: Prospects for Therapeutics. *Curr. Opin. Chem. Biol.* **2001**, *5*, 416–423.
(7) Barford, D.; Jia, Z.; Tonks, N. K. Protein Tyrosine Phosphatases Take Off. *Nat. Struct. Biol.* **1995**, *2*, 1043–1053.
(8) Fauman, E. B.; Saper, M. A. Structure and Function of the Protein Tyrosine Phosphatases. *Trends Biochem. Sci.* **1996**, *21*, 413–417.
(9) Salmeen, A.; Andersen, J. N.; Myers, M. P.; Tonks, N. K.; Barford, D. Molecular Basis for the Dephosphorylation of the Activation Segment of the Insulin Receptor by Protein Tyrosine Phosphatase 1B. *Mol. Cell* **2000**, *6*, 1401–1412.
(10) Elchebly, M.; Payette, P.; Michaliszyn, E.; Cromlish, W.; Collins, S.; Loy, A. L.; Normandin, D.; Cheng, A.; Himms-Hagen, J.; Chan, C. C. Increased Insulin Sensitivity and Obesity Resistance in Mice Lacking the Protein Tyrosine Phosphatase-1B Gene. *Science* **1999**, *283*, 1544–1548.
(11) Klaman, L. D.; Boss, O.; Peroni, O. D.; Kim, J. K.; Martino, J. L.; Zabolotny, J. M.; Moghal, N.; Lubkin, M.; Kim, Y. B.; Sharpe, A. H. Increased Energy Expenditure, Decreased Adiposity, and Tissue-Specific Insulin Sensitivity in Protein-Tyrosine Phosphatase 1B-Deficient Mice. *Mol. Cell. Biol.* **2000**, *20*, 5479–5489.
(12) Barford, D.; Flint, A. J.; Tonks, N. K. Crystal Structure of Human Protein Tyrosine Phosphatase 1B. *Science* **1994**, *263*, 1397–1404.
(13) Kamerlin, S. C. L.; Rucker, R.; Boresch, S. A. Molecular Dynamics Study of WPD-Loop Flexibility in PTP1B. *Biochem. Biophys. Res. Commun.* **2007**, *356*, 1011–1016.
(14) Jia, Z.; Barford, D.; Flint, A. J.; Tonks, N. K. Structural Basis for Phosphotyrosine Peptide Recognition by Protein Tyrosine Phosphatase 1B. *Science* **1995**, *268*, 1754–1758.
(15) Pedersen, A. K.; Guo, X. L.; Moller, K. B.; Peters, G. H.; Andersen, H. S.; Kastrup, J. S.; Mortensen, S. B.; Iversen, L. F.; Zhang, Z. Y.; Moller, N. Residue 182 Influences the Second Step of Protein-Tyrosine Phosphatase-Mediated Catalysis. *Biochem. J.* **2004**, *378*, 421–434.
(16) Ala, P. J.; Gonneville, L.; Hillman, M.; Becker-Pasha, M.; Yue, E. W.; Douty, B.; Wayland, B.; Polam, P.; Crawley, M. L.; McLaughlin, E. Structural Insights into the Design of Nonpeptidic Isothiazolidinone-Containing Inhibitors of Protein-Tyrosine Phosphatase 1B. *J. Biol. Chem.* **2006**, *281*, 38013–38021.
(17) Wiesmann, C.; Barr, K. J.; Kung, J.; Zhu, J.; Erlanson, D. A.; Shen, W.; Fahr, B. J.; Zhong, M.; Taylor, L.; Randal, M. Allosteric Inhibition of Protein Tyrosine Phosphatase 1B. *Nat. Struct. Mol. Biol.* **2004**, *11*, 730–737.
(18) Frimurer, T. M.; Peters, G. H.; Iversen, L. F.; Andersen, H. S.; Møller, N. P. H.; Olsen, O. H. Ligand-Induced Conformational Changes: Improved Predictions of Ligand Binding Conformations and Affinities. *Biophys. J.* **2003**, *84*, 2273–2281.
(19) Wilson, D. P.; Wan, Z. K.; Xu, W. X.; Kirincich, S. J.; Follows, B. C.; Joseph-McCarthy, D.; Foreman, K.; Moretto, A.; Wu, J.; Zhu, M. Structure-Based Optimization of Protein Tyrosine Phosphatase 1B Inhibitors: From the Active Site to the Second Phosphotyrosine Binding Site. *J. Med. Chem.* **2007**, *50*, 4681–4698.
(20) Sun, J. P.; Fedorov, A. A.; Guo, X.; Lee, S. Y.; Guo, X. L.; Shen, K.; Lawrence, D. S.; Alom, S. C.; Zhang, Z. Y. Crystal Structure of PTP1B Complexed with a Potent and Selective Bidentate Inhibitor. *J. Biol. Chem.* **2003**, *278*, 12406–12414.
(21) Sussman, J. L.; Lin, D.; Jiang, J.; Manning, N. O.; Prilusky, J.; Ritter, O.; Abola, E. E. Protein Data Bank (PDB): Database of Three-Dimensional Structural Information of Biological Macromolecules. *Acta Crystallogr., Sect. D: Biol. Crystallogr.* **1998**, *54*, 1078–1084.
(22) Sali, A.; Blundell, T. L. Comparative Protein Modelling by Satisfaction of Spatial Restraints. *J. Mol. Biol.* **1993**, *234*, 779–815.
(23) DeLano, W. L. *The PyMOL Molecular Graphics System*; DeLano Scientific: San Carlos, CA, 2002.
(24) *SYBYL*, version 7.1; Tripos International: St. Louis, MO, 2005.
(25) Morris, G. M.; Goodsell, D. S.; Halliday, R. S.; Huey, R.; Hart, W. E.; Belew, R. K.; Olson, A. J. Automated Docking Using a Lamarckian Genetic Algorithm and an Empirical Binding Free Energy Function. *J. Comput. Chem.* **1998**, *19*, 1639–1662.
(26) Frisch, M. J.; Trucks, G. W.; Schlegel, H. B.; Scuseria, G. E.; Robb, M. A.; Cheeseman, J. R.; Montgomery, J. A.; Vreven, T. ; K. N. K.; Burant, J. C.; Millam, J. M.; Iyengar, S. S.; Tomasi, J.; Mennucci, V. B.; Cossi, M.; Scalmani, G.; Rega, N.; Petersson, G. A.; Nakatsuji, H.; Hada, M.; Ehara, M.; Toyota, K.; Fukuda, R.; Hasegawa, J.; Ishida, M.; Nakajima, T.; Honda, Y.; Kitao, O.; Nakai, H.; Klene, M.; Li, X.; Knox, J. E.; Hratchian, H. P.; Cross, J. B.; Bakken, V.; Adamo, C.; Jaramillo, J.; Gomperts, R.; Stratmann, R. E.; Yazyev, O.; Austin, A. J.; Cammi, R.; Pomelli, C.; Ochterski, J. W.; Ayala, P. Y.; Morokuma, K.; Voth, G. A.; Salvador, P.; Dannenberg, J. J.; Zakrzewski, V. G.; Dapprich, S.; Daniels, A. D.; Strain, M. C.; Farkas, O.; Malick, D. K.; Rabuck, A. D.; Raghavachari, K.; Foresman, J. B.; Ortiz, J. V.; Cui, Q.; Baboul, A. G.; Clifford, S.; Cioslowski, J.; Stefanov, B. B.; Liu, G.; Piskorz, A.; P.; Komaromi, I.; Martin, R. L.; Fox, D. J.; Keith, T.; Al-Laham, M. A.; Peng, C. Y.; Nanayakkara, A.; Challacombe, M.; Gill, P. M. W.; Johnson, B.; Chen, W.; Wong, M. W.; Gonzalez, C.; and Pople, J. A. *Gaussian 03*, revision C.02; Gaussian Inc.: Wallingford, CT, 2004.
(27) Bayly, C. I.; Cieplak, P.; Cornell, W. D. K. A Well-Behaved Electrostatic Potential Based Method Using Charge Restraints for Deriving Atomic Charges: the RESP Model. *J. Phys. Chem.* **1993**, *97*, 10269–10280.
(28) Cornell, W. D.; Cieplak, P.; Bayly, C. I.; Gould, I. R.; Merz, K. M.; Ferguson, D. M.; Spellmeyer, D. C.; Fox, T.; Caldwell, J. W.; Kollman, P. A. A Second Generation Force Field for the Simulation of Proteins, Nucleic Acids, and Organic Molecules. *J. Am. Chem. Soc.* **1995**, *117*, 5179–5197.
(29) Wang, J.; Wolf, R. M.; Caldwell, J. W.; Kollman, P. A.; Case, D. A. Development and Testing of a General Amber Force Field. *J. Comput. Chem.* **2004**, *25*, 1157–1174.
(30) Case, D. A.; Darden, T. A.; Cheatham, I., T.E.; Simmerling, C. L.; Wang, J.; Duke, R. E.; Luo, R.; Crowley, M.; Walker, R. C.; Zhang, W.; Merz, K. M.; Wang, B.; Hayik, S.; Roitberg, A.; Seabra, G.; Kolossváry, I.; Wong, K. F.; Paesani; J. Vanicek, F.; Wu, X.; Brozell, S. R.; Steinbrecher, T.; Gohlke, H.; Yang, L.; Tan, C.; Mongan, J.; Hornak, V.; Cui, G.; Mathews, D. H.; Seetin, M. G.; Sagui, C.; Babin, V.; Kollman, P. A. *AMBER*, version 10; University of California: San Francisco, CA, 2008.
(31) Lohse, D. L.; Denu, J. M.; Santoro, N.; Dixon, J. E. Roles of Aspartic Acid-181 and Serine-222 in Intermediate Formation and Hydrolysis of the Mammalian Protein-Tyrosine-Phosphatase PTP1B. *Biochemistry* **1997**, *36*, 4568–4575.
(32) Peters, G. H.; Frimurer, T. M.; Andersen, J. N.; Olsen, O. H. Molecular Dynamics Simulations of Protein-Tyrosine Phosphatase 1B. I. Ligand-Induced Changes in the Protein Motions. *Biophys. J.* **1999**, *77*, 505–515.
(33) Peters, G. H.; Frimurer, T. M.; Andersen, J. N.; Olsen, O. H. Molecular Dynamics Simulations of Protein-Tyrosine Phosphatase 1B. II. Substrate-Enzyme Interactions and Dynamics. *Biophys. J.* **2000**, *78*, 2191–2200.
(34) Jorgensen, W. L.; Chandrasekhar, J. M.; Jd, I. RW; Klein, M. L. Comparison of Simple Potential Functions for Simulating Liquid Water. *J. Chem. Phys.* **1983**, *79*, 926–935.
(35) Van Gunsteren, W. F.; Berendsen, H. J. C. Algorithms for Macromolecular Dynamics and Constraint Dynamics. *Mol. Phys.* **1977**, *34*, 1311–1327.
(36) Darden, T.; York, D.; Pedersen, L. Particle Mesh Ewald: An N.Log (N) Method for Computing Ewald Sums. *J. Chem. Phys.* **1993**, *98*, 10089–10092.
(37) Humphrey, W.; Dalke, A.; Schulten, K. VMD. Visual Molecular Dynamics. *J. Mol. Graphics* **1996**, *14*, 33–38.
(38) Cheatham 3rd, T. E.; Srinivasan, J.; Case, D. A.; Kollman, P. A. Molecular Dynamics and Continuum Solvent Studies of the Stability of Polyg-Polyc and Polya-Polyt DNA Duplexes in Solution. *J. Biomol. Struct. Dyn.* **1998**, *16*, 265–280.
(39) Kuhn, B.; Kollman, P. A. Binding of a Diverse Set Of Ligands to Avidin and Streptavidin: an Accurate Quantitative Prediction of Their Relative Affinities by a Combination of Molecular Mechanics and Continuum Solvent Models. *J. Med. Chem.* **2000**, *43*, 3786–3791.
(40) Massova, I.; Kollman, P. A. Combined Molecular Mechanical and Continuum Solvent Approach (MM-PBSA/GBSA) to Predict Ligand Binding. *Perspect. Drug Discovery Des.* **2000**, *18*, 113–135.
(41) Tsui, V.; Case, D. A. Theory and Applications of the Generalized Born Solvation Model in Macromolecular Simulations. *Biopolymers* **2001**, *56*, 276–291.
(42) Still, W. C.; Tempczyk, A.; Hawley, R. C.; Hendrickson, T. Semianalytical Treatment of Solvation for Molecular Mechanics and Dynamics. *J. Am. Chem. Soc.* **1990**, *112*, 6127–6129.
(43) Gohlke, H.; Case, D. A. Converging Free Energy Estimates: MM-PB (GB) SA Studies on the Protein-Protein Complex Ras-Raf. *J. Comput. Chem.* **2004**, *25*, 238–250.
(44) Gohlke, H.; Kiel, C.; Case, D. A. Insights into Protein-Protein Binding by Binding Free Energy Calculation and Free Energy Decomposition for the Ras-Raf and Ras-Ralgds Complexes. *J. Mol. Biol.* **2003**, *330*, 891–913.
(45) Northrup, S. H.; Pear, M. R.; McCammon, J. A.; Karplus, M. Molecular Dynamics of Ferrocytochrome C. *Nature* **1980**, *286v, 1?*>, 304–305.

(46) Northrup, S. H.; Pear, M. R.; McCammon, J. A.; Karplus, M.; Takano, T. Internal Mobility of Ferrocytochrome C. *Nature* **1980**, *287*, 659–660.
(47) Bharatham, K.; Bharatham, N.; Kwon, Y. J.; Lee, K. W. Molecular Dynamics Simulation Study of PTP1B with Allosteric Inhibitor and its Application in Receptor Based Pharmacophore Modeling. *J. Comput.-Aided Mol. Des.* **2008**, *22*, 925–933.
(48) Wang, J.; Gong, K.; Wei, D.; Li, Y.; Chou, K. Molecular Dynamics Studies on the Interactions of PTP1B with Inhibitors: From the First Phosphate-Binding Site to the Second One. *Protein Eng., Des. Sel.* **2009**, *22*, 349–355.
(49) Zhang, X.; Li, X.; Wang, R. Interpretation of the Binding Affinities of PTP1B Inhibitors with the MM-GB/SA Method and the X-Score Scoring Function. *J. Chem. Inf. Model.* **2009**, *49*, 1033–1048.

CI900484G